International Journal of Technology 14(1) 65-77 (2023)
Received September 2021 / Revised January 2022 / Accepted July 2022

International Journal of Technology

Optoelectronic Characterization and Properties of Single-walled Carbon Nanotubes in a Liquid Dispersion Form

Sami S. Alabsi[1*], Mohd Haris Md. Khir[1], John Ojur Dennis[2], Saeed S. Ba Hashwan[1], Abdullah S. Algamili[1]

[1]*Department of Electrical and Electronic Engineering, Universiti Teknologi PETRONAS, Seri Iskandar 32610, Malaysia*
[2]*Department of Fundamental and Applied Sciences, Universiti Teknologi PETRONAS, Seri Iskandar 32610, Malaysia*

Abstract. Carbon nanotubes (CNTs) are very promising nanodevices due to their extraordinary electrical, thermal, and optical properties. However, as-grown single-walled CNTs (SWCNTs) contain a mixture of semiconducting and metallic species with great features versatility and variation. Solution-based processing of this nanomaterial is vital for further implementation in applicable platforms. In this paper, important optoelectronic intrinsic properties of SWCNTs in dispersions are studied applying a semi-empirical approach of optical characterization and Tauc/Davis-Mott relation and Max-Planck equations. SWCNTs are found to have a direct bandgap of 2.20 eV, an indirect bandgap of 0.27 eV, an optical conductivity of about 10^7 S cm^{-1}, and exhibited a metamaterial behavior ascribed to the high negative permittivity. In addition, the optimum parameters for the dispersion of SWCNTs, and the separation of the semiconducting species using simple mechanical methods of ultrasonication and density gradient ultracentrifugation, respectively, without using surfactants are also presented.

Keywords: Carbon nanotubes; Dispersion; Optoelectronic properties; Separation; Spectroscopy

1. Introduction

CNTs are allotropes of the carbon family with hollow cylinder structures. Based on the chirality angle divergence of the graphene sheet, their electronic properties may vary between metallic and semiconducting CNTs exist as single-walled, dual-walled or multiwalled (Setyopratomo *et al.,* 2018; Thanthirige *et al.,* 2016). Consisting only of surface (i.e., no bulk C-atoms), they are extremely sensitive and responsive to surface modification and optical excitation. This peculiarity of 1D ultra-thin structure renders CNTs as a potential material for future high-performance scaled nanotechnology (Alabsi *et al.,* 2020; Sudibandriyo *et al.,* 2015). The optoelectronic properties of SWCNTs are important features and determinants of many applications of these nanodevices.

Optoelectronic applications of SWCNTs are increasingly gaining more attention due to the extreme sensitivity and responsivity of these nanodevices to light energy. Absorption of light observes the momentum and energy conservation laws which imply that the photo-

*Corresponding author's email: sami_18001518@utp.edu.my, Tel.: 006-0192525125
doi: 10.14716/ijtech.v14i1.5124

energy sufficient for the excitation of electrons from ground Anomalous optoelectronic behavior of SWCNTs may, however, be associated with structural defects and/or surface functionalization.

Thus, spectroscopy of the intrinsic properties of pristine SWCNTs is fathomable by analysis in the range of UV-Vis and NIR spectra. In fact, optical characterization is the preferred technique and is perhaps the simplest method of studying the intrinsic properties of dispersion based SWCNTs (Eremina *et al.,* 2017; Cheung *et al.,* 2016; Nguyen and Shim, 2015;). It paves the way for their implementation in many optoelectronic applications (Mousavi, 2012). It is also a tool to investigate the phases of several processes in real time, such as the quality of the dispersion and separation of metallic and semiconducting nanotubes (Yang *et al.,* 2016). Optical analysis may reveal numerous optoelectronic properties of SWCNTs such as optical transmittance (Tsapenko *et al.,* 2018), conductivity and dielectric properties (Smirnov *et al.,* 2019; Smirnov *et al.,* 2018), energy bandgap, and optical absorption coefficient (El-Moussawi *et al.,* 2019; Saad *et al.,* 2019; Blancon *et al.,* 2015).

Intriguingly, SWCNTs exhibit extraordinary but anisotropic properties. This anisotropicity stems from the nanotubes variation in several factors such as diameter, chirality, and length (Sharma and Jaggi, 2017; Ba Hashwan *et al.,* 2015). Despite numerous studies on the optical and electronic characteristics of SWCNTs, knowledge of their optoelectronic conductivity, bandgap energy, and dielectric behavior is still a matter of ongoing research. For instance, Mousavi reported that larger SWCNT diameter is associated with lower bandgaps and hence higher optical conductivity (Mousavi, 2012). Kuwahara, Hirai, and Saito (2018), on the other hand, demonstrated that a thin film SWCNTs network of smaller diameter tubes showed better conductivity performance. Length of the nanotube may also be a factor determining the optoelectronic features of the SWCNTs. Shorter tubes are associated with less light transmittance and lower conductivity (Farbod, Zilaie, Kazeminezhad, 2017). He *et al.* (2016) reported an extremely anisotropic conductivities of perpendicularly (~42 Scm^{-1}) and parallelly (~2500 Scm^{-1}) aligned SWCNTs electronic devices. The bandgap of the nitrophenyl functionalized SWCNTs was calculated between 1.19 eV and 2.60 eV by (El-Moussawi *et al.,* 2019). Kawale *et al.* (2016) obtained an average bandgap of 1.23 eV for samples synthesized at 700° C, while reporting a nearly 0 eV indirect bandgap for all carbon films. On the contrary, a large window of a direct bandgap of 6 eV and indirect bandgap of 5.2 eV of pristine CNTs was reported by (Murali and Perumal, 2018). Nonetheless, the absorption spectra have shown some variation over several studies. In one study, the UV-Vis absorption peaks of SWCNTs solution were reported at 225 nm and 273 nm (Attal, Thiruvengadathan, and Regev, 2006), while absorption maxima were observed at ~206 nm and ~251 nm by another study (Rance *et al.,* 2010). π-plasmon absorption with two extreme peaks at ~246 and ~275 nm were recorded by (Cheung *et al.,* 2016).

Even though SWCNTs have received much attention in the past decade, their properties are still being a subject of intense research. This article presents the first comprehensive study to investigate the important optoelectronic properties, namely, the optical absorbance, energy bandgap, optoelectronic conductivity, and the dielectric behaviour of pristine SWCNTs utilizing a semi-empirical approach of optical characterization and Beer-Lambert law (Chiodarelli and De Volder, 2019; Njuguna, Vanli, and Liang, 2015), Tauc and Davis-Mott relation (Berwal *et al.,* 2017; Johan *et al.,* 2014; Kim *et al.,* 2014; Tan *et al.,* 2012; Li *et al.,* 2009) and Max-Planck equations (Bouazza *et al.,* 2021; Arbab, 2019). Interestingly, the analysis of the optical absorbance of the samples prepared for the optical characterization revealed significant results about the nanotubes dispersion and separation. Simple mechanical methods of dispersion and separation were followed in preparing the

SWCNTs samples, while avoiding the use of surfactants to preserve the intrinsic properties of the nanotubes for more reliable optical characterization. Supported by semi-empirical results, optical characterization has shown that separation of SWCNTs is achievable with repetitive cycles of sonication and ultracentrifugation at a certain relative gravity force (RCF) with careful extraction and yield fractioning.

2. Materials and Methods

2.1. Materials

The materials used in this study were of analytical grade. Pristine unfunctionalized SWCNTs in powder form produced by arc-discharge technique was obtained from Iljin Nanotech. The polar solvents of dimethyl formamide (DMF) and tetrahydrofuran (THF), and DI water (18.2 MΩ cm) were purchased from Sigma-Aldrich. All materials were used as received. Experiments were conducted at the nanomaterials laboratory, Universiti Teknologi Petronas.

2.2. Methodology

2.2.1. Dispersion and separation

Solution based SWCNTs was prepared by adding the powder form of pristine as-synthesized SWCNTs to DMF in three different concentrations: 0.1%, 0.01%, and 0.001% ω/v. The mixture was then ultrasonicated, using Jeken ultrasonicator PS-40A, at four different sonication durations: 30min, 60min, 90min, and 120min, at a moderate power of 40W. The use of surfactants was avoided to preserve the intrinsic properties of the nanotubes.

For the separation of the semiconduction (sc)-CNTs from the metallic (m)-CNTs, 0.01% w/v aqueous solution of SWCNTs in DI water was stirred at 300 rpm for 30 min at room temperature, then ultracentrifuged at 15,000 rpm ~ 27720 RCF, using Benchtop High Speed Refrigerated Centrifuge BCBHR-308, at four different cycle and duration settings: 30 min, 60 min, 90 min, 120 min. The supernatant yield was carefully fractioned for optical analysis after each centrifugation cycle. The algorithm is related to the density gradience between the two electronic species with the semiconducting being buoyant with less dense gradient extracted from the top phase of the yield. In other words, ultracentrifugation at this gravity force might be effective in the separation of nanotubes suggesting gradient of metallic nanotubes is denser than semiconducting ones.

2.2.2. Characterization

Spectroscopy of absorbance/reflectance of light in the ultraviolet, visible and near infrared regions was performed using UV-Vis NIR spectroscopy (Agilant, Carry 60) with a dual beam mode, a scan rate of 4800 nm/min, starting wavelength of 1100 nm and a stopping wavelength of 190 nm. Correction/subtraction of the blank spectra (i.e., DMF solvent) from the sample by dual-beam spectrometer was reckoned for to obtain the absorbance due purely to the CNT species.

3. Results and Discussion

3.1. Absorption Spectra and Dispersion

The transition that occurs from the ground state to the excited state requires the absorption of a specific amount of energy given by $E = hv$, where h is the Planck's constant and v is the frequency of the incident light.

The energy difference between HOMO and LUMO corresponds to the electron excitations pertaining to absorption of a specific light wavelength spectrum. The broad

range of wavelengths in Figure 1 is, in fact, explained by the CNT 1D structure density of states known as Van Hove singularities. The transition that takes place at the wavelength that absorbs most strongly at 275 nm for 0.1% concentration, and at 280 nm for both 0.01% and 0.001% concentrations represent the π-plasmon absorbance.

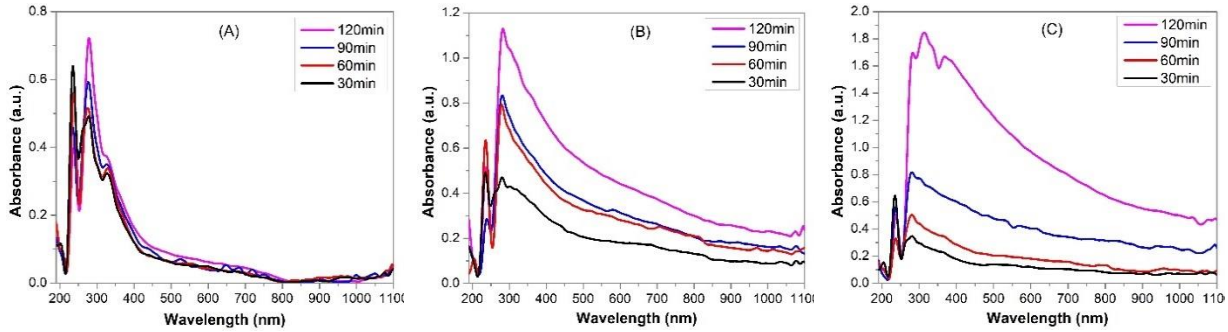

Figure 1 Absorbance spectra relative to variation of sonication durations against variation of concentration: (A) 0.1%, (B) 0.01%, and (C) 0.001% of SWCNT/DMF.

The increase in sonication time had a significant effect on increasing the absorbance intensity in all concentrations. At the highest concentration of 0.1%, the increase of absorbance intensity over sonication durations was somehow monotonic. Lower concentrations had higher rate of SWCNTs deagglomeration evident by the increment in the absorbance intensities. Dramatic increase, however, takes place at 120 min/0.01%, 90 min/0.001% and even more sizable leap is observable at 120 min/0.001% reaching as much as double the absorbance intensity as that of 120 min/0.1%. Higher absorbance intensities signify higher rate of debundling and homogeneity of the dispersions (Nguyen *et al.,* 2011). The absorbance is remarkably showing two significant peaks: small and major. The major absorbance peak of 0.1% occurs at 275 nm but a shift towards the red zone is observed as concentration decreases with peaks center at 280 nm for 0.01% and 0.001%. The small peak at 236 nm remains unshifted regardless of the change in concentration and sonication duration. The major peaks represent the strong π-plasmon resonance absorbance peaks of the nanotubes in liquid form (Smirnov *et al.,* 2019). Similar strong π-plasmon peaks were observed by (Li *et al.,* 2009). Table 1 demonstrates the prominent peaks along with their respective wavelengths for all concentrations and sonication durations.

Table 1 Absorbance intensities and corresponding wavelengths of major peaks for each duration setting and concentration

		30 min		60 min		90 min		120 min			
		1st peak	2nd peak	1st peak	2nd peak	1st peak	2nd peak	1st peak	2nd peak	3rd peak	4th peak
0.001 %	Abs	~ 0.55	~ 0.8	~ 0.65	~ 0.4	~ 0.35	~ 0.45	~ 0.50	~ 1.7	~ 1.9	~ 1.7
	λ	236	280	236	280	236	280	236	280	310	370
0.01%	Abs	~ 0.50	~ 0.50	~ 0.65	~ 0.8	~ 0.30	~ 0.85	~ 0.50	~ 1.10	-	-
	λ	236	280	236	280	236	280	236	280	-	-
0.1%	Abs	~ 0.45	~ 0.60	~ 0.65	~ 0.50	~ 0.55	~ 0.50	~ 0.40	~ 0.70	-	-
	λ	236	275	236	275	236	275	236	275	-	-

Monotonic decrease in absorbance intensity after the major peak of 0.1% and 0.01% is observed without showing further significant isolated peaks. Note that only after

120min/0.001% the major peak is now contorted to include two more peaks. The inclusion of the two peaks of 310 nm and 370 nm, along with the significant increase in the absorbance intensities, especially at 120 min, is an indication of a deeper and more significant deagglomeration of the SWCNTs and confirms that the dispersion has improved over sonication durations.

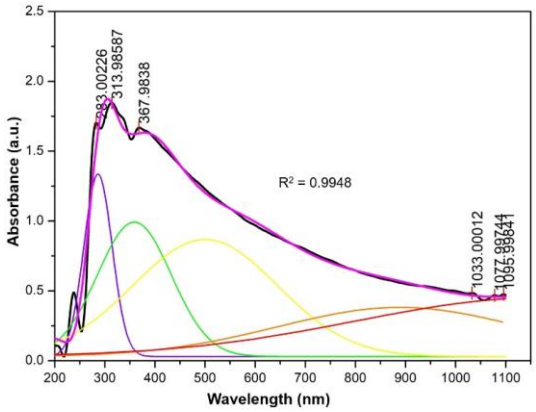

Figure 2 Deconvolution of the 120 min/0.001% setting peak

The interband excitonic transitions are more evident and wider, which implies higher rate of deagglomeration and the existence of individually dispersed SWCNTs at higher rates in the lower concentration dispersions, specifically at the highest sonication duration of 120 min than in the higher concentrations and at lower sonication durations. The deconvolution analysis of the highest peak of the 120 min/0.001% setting in Figure 2 illustrates the breakdown of the individual nanotube transitions. It reveals the mixture composition and the variation of the nanotubes' properties between metallic and semiconducting as the absorption shifts from the UV to the visible and near infrared regions. The increment in the absorbance intensities is also an indication of better dispersibility and debundling of individual nanotubes over extended sonication durations (Jiang, Song, and Xu, 2018). Moreover, the few peaks along the wavelength spectrum is an indication of the purity of the nanotube species and the low rate of contamination.

However, DMF is a neutral Lewis base that readily facilitates the catalysis of the reversible process of deprotonation of the nanotubes (Arai, 2010). The shift in the peak waveform towards the NIR zone may also be an indication of the deprotonation of the carbon nanotubes with longer sonication durations (Kozlowska, Meyer, and Rodziewicz, 2019; Nguyen and Shim, 2015). It can also be ascribed to the swelling, ionization, and dissociation of the nanotube species in the DMF. While metallic SWCNTs are more reactive to protonation near neutral pH, semiconducting SWCNTs are reactive and sensitive to protonation near more acidic pH values (Engtrakul *et al.,* 2005). Protonation is a reversible process whereby SWCNTs neither lose their electron, nor do they change structure of electronic state permanently.

Absorbance spectra presented here, are in accordance with the results obtained by (El-Moussawi *et al.,* 2019). Similar waveforms were also observed in other works (Nguyen and Shim, 2015; Nguyen *et al.,* 2011).

In comparison, other studies reported longer sonication durations, and some resorted to the use of surfactants which are difficult to remove and known to degrade the performance of the nanotubes. Mougel *et al.* (2016) reported the successful dispersion of SWCNTs at an optimum sonication time of 2.5 h using a power density of 0.7 W/mL. Another study showed that SWCNTs retained most of their length after 2 h sonication of the nanotubes in SDBS at 90 W (Gomulya *et al.,* 2013). At a higher power of 225 W, Barman *et*

al. (2010) investigated the optical characteristics of SWCNTs in NMP at a range of different sonication durations reaching up to 480 min. The absorption intensity increased and peaked at 120 min but notably decreased after this duration point due to re-bundling that was confirmed by AFM images. While in a different study, a tip-sonication was performed to disperse SWCNTs in sodium deoxycholate (DOC) for 1.5 h in an ice water bath at a power of 1 W/mL. Raman analysis of the nanotubes lengths indicated a low level of defects (Simien *et al.,* 2008).

3.2. Separation of sc-SWCNTs

The optical absorption bands of the sc-SWCNTs buoyant density fraction is illustrated in Figure 3. Isolated nanotubes absorb light at different wavelengths allowing for the determination of their conductivity type. The photoresponse of the metallic (M_{11}) electronic transition is observed in the visible region, while the photoresponse of the semiconducting (S_{22}) electronic transition of the nanotubes is observed in the near infrared region (Ong, Euler, and Levitsky, 2010). The complete attenuation of the absorption spectra at the M_{11} transition band of the metallic nanotubes and the notable increase in the absorption spectra at the S_{22} transition band of semiconducting nanotubes is an indication of the successful separation of the sc-CNTs from m-CNTs. Notably, the absorption peaks of the metallic nanotubes transition bands faded away with longer DGU durations, while absorption peaks at the semiconducting absorption band gained stronger pulse at higher DGU durations. Fractions after each ultracentrifugation setting contained higher purity yield of semiconducting nanotubes. This is evident by the inclusion of more peaks with higher intensities at the S_{22} excitonic band and the demise of the peaks at the M_{11} excitonic band due to the consistent increasing rate of gradient buoyancy density differentiation of the sc-CNTs and the m-CNTs with increased ultracentrifugation duration settings. Absorbance peaks in the S_{22} excitonic band are attributed to the Van Hove singularities absorption in the NIR region. Results here are in agreement with results by (Wang and Lei, 2020; Tang *et al.,* 2018; Eremina *et al.,* 2017).

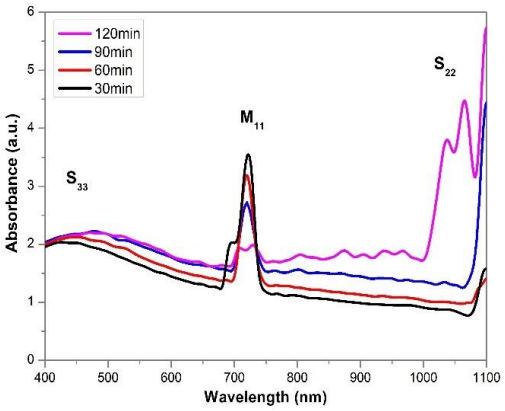

Figure 3 Metallic and semiconducting electronic transitions

The separation of the sc-SWCNTs from the m-SWCNTs was further validated by the extrapolation of the bandgap energies discussed in following section.

3.3. Bandgap

The bandgap of a material is the difference of energy that an electron is required to have in order to make a transition from one band of lower energy to another of higher energy. Based on the energy required to make this transition, the absorption of photo-energy in the UV-Vis NIR spectroscopy is correspondent to specific molecular orbitals (MO). As aforementioned, these orbitals represent bonding and antibonding orbitals, and the

transition takes place between the HOMO and the LUMO. The absorption at the red edge of the spectra is utilized to determine the bandgap. The bandgap is obtained using equation:

$$(ahv)^n = K(hv - E_g) \quad (1)$$

where α is the absorbance coefficient, and the collective term (hv) is denoting the incident photon energy. The exponent "n" represents the nature of transition. For direct transition, $n = 2$, and for indirect transition, $n = ½$. K is energy independent constant, and E_g is the optical bandgap energy.

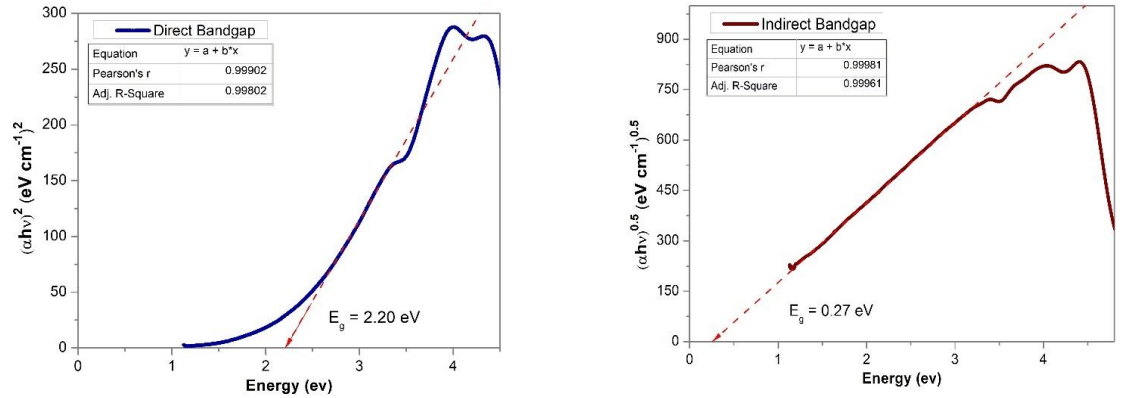

(a) Before DGU

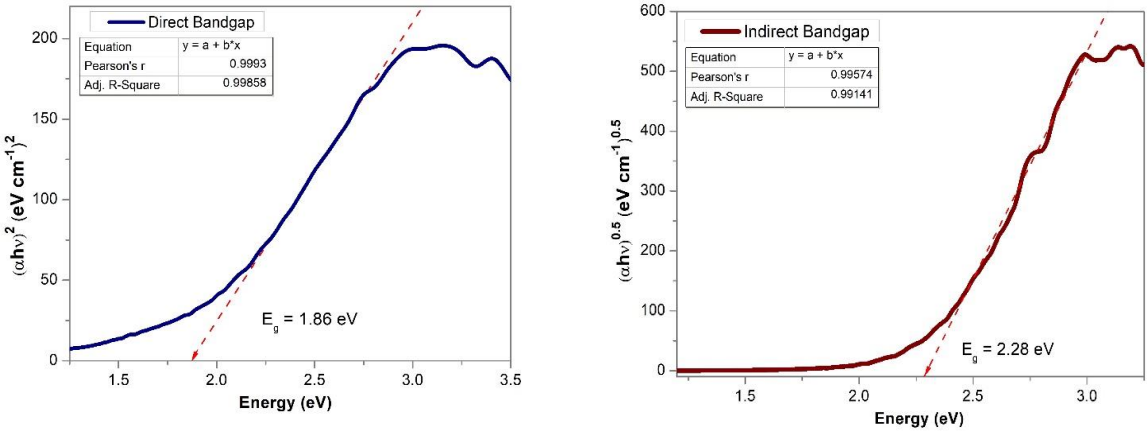

(b) After DGU

Figure 4 Tauc-Davis Mott direct and indirect band gap transitions for (A) before and (B) after DGU

The extrapolation of the bandgaps in Figure 4 demonstrates that SWCNTs are direct and indirect nanomaterial. There is a significant disparity between the direct bandgap and the indirect one obtained from the samples before DGU. This is ascribed to the nature of the as-synthesized nanotubes having a mixture of both metallic and semiconducting species.

The indirect bandgap at 0.27 eV is showing a quasi-metallic behavior of the nanotubes, while the 2.20 eV direct bandgap is more to the semiconducting nano-species, both existing in the as-synthesized mixture. The bandgap is inversely proportional to the nanotube diameter. A 2.20 eV bandgap might be associated to a CNT with a diameter of a 0.2 nm, while a small bandgap could be of a CNT with a larger diameter (Venkataraman *et al.*, 2019).

However, after the DGU, the direct and indirect bandgap disparity has significantly shrunken, and the difference was reduced to a lower range. In Figure 4, the values of 1.86 eV and 2.28 eV, for the direct and indirect bandgaps, respectively, are both in the semiconducting range, which is believed to be due to the separation of the metallic nanotubes from the semiconducting ones.

Indirect bandgap of CNTs was reported by one study (Wang *et al.,* 2017). SWCNTs may change, under strain, from direct to indirect gaps as explained by (Qiu *et al.,* 2016). While, another study construed that the nanotubes are of direct bandgap due to their 1D structure (Li *et al.,* 2009). Murali and Perumal (2018) extrapolated the bandgap of SWCNT at 6 eV and 5.2 eV for direct and indirect transitions, respectively, using x-intercept in Tauc plot.

According to a probable direct inter-band transitions between the Van Hove singularities and the density of states, three optical bandgaps of 2.2 eV, 3.5 eV, and 4 eV were obtained by (Gharbavi and Badehian, 2015). In another study based on density functional methods, it was showed that armchair (n, n) SWCNTs have indirect semiconducting bandgap ranging 1.062 eV - 2.112 eV (n = 3 – 10), while for zigzag (n, 0), the SWCNTs have a direct semiconducting bandgap ranging 0.659 eV - 1.603 eV (n = 5 – 10) (Sun, 2011).

3.3. Optical Conductivity

Optical conductivity is another important parameter in the optoelectronic analysis of CNTs. It unlocks the potential for numerous applications of CNTs in optoelectronic field (Mousavi, 2012). The optical conductivity (σ_{opt}) was mathematically modelled and graphed against the excitation wavelengths and against the incident photon energy.

Optical conductivity σ_{opt} depends mainly on the optical bandgap, refractive index, absorption coefficient, incident photon frequency and excitation coefficient and is given by the following equation (Arbab, 2019; Sharma and Katyal, 2007):

$$\sigma_{opt} = \frac{\alpha n c}{4\pi} \tag{2}$$

where n is the refractive index, and c is the speed of light in vacuum. The refractive index is given by:

$$n = \frac{1}{T_s} + \sqrt{\frac{1}{T_s - 1}} \tag{3}$$

where $T_s = 10^{(-A)} \times 100$ is the percentage of transmittance, and A is the light absorbance, which is a dimensionless quantity.

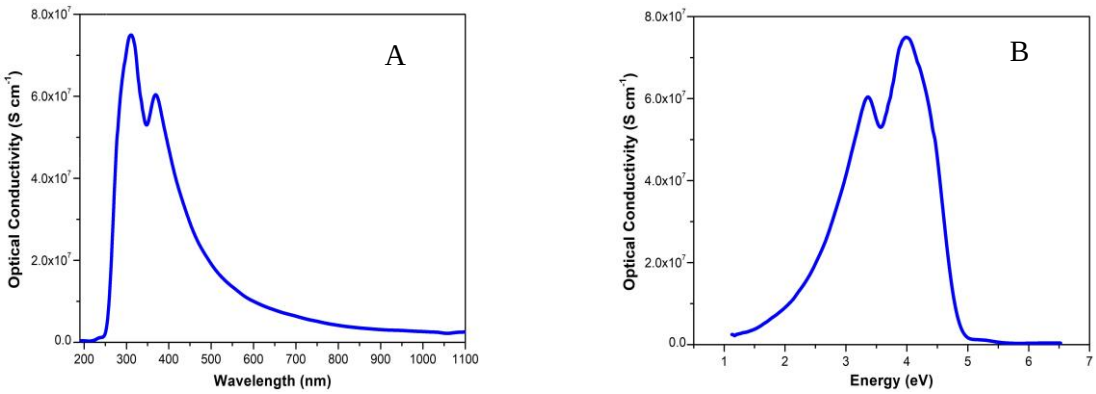

Figure 5 Optical conductivity of SWCNTs as a function of (A) wavelength and (B) optical energy

Figure 5 depicts the optical conductivity of the SWCNTs. The most prominent peak centers at ~3.9 eV, similar to results reported by (Gharbavi and Badehian, 2015). Another smaller peak at ~3.35 eV is also evident. This means that SWCNTs are most conducting at optical energy bands of ~3.35 - 3.9 eV. Moreover, it is observed that the maxima of electron excitation are attained at wavelengths 310 nm and 370 nm. SWCNTs have a high conductivity in the order of 10^7 - 10^8 as also reported by (Venkataraman *et al.,* 2019; Zhang

et al., 2015). While, a non-resonant optical conductivity of individual SWCNTs was measured at $(6 \pm 1) \times 10^{-5} \Omega^{-1}$ by another study (Blancon *et al.,* 2015).

3.4. Dielectric

The dielectric behavior of SWCNTs is given by $\varepsilon_r = n^2 - k^2$, and $\varepsilon_i = 2nk$, where ε_r and ε_i are the dielectric constant real and imaginary parts, respectively. n is the refractive index. K is the extinction coefficient, and α is the absorption coefficient obtained by the following equations:

$$K = \frac{\alpha\lambda}{4\pi} \tag{4}$$

$$\alpha = \frac{2.303 \times A}{l} \tag{5}$$

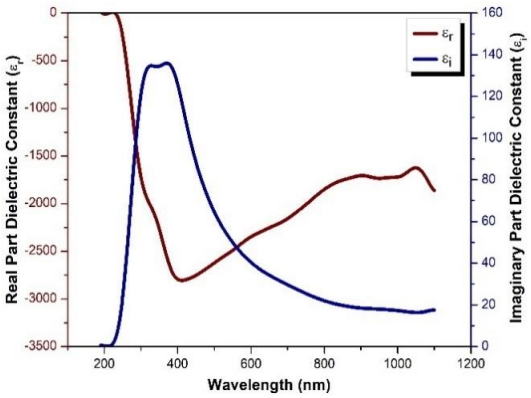

Figure 6 The real and the imaginary parts of SWCNTs dielectric behavior

The permittivity properties of the nanotubes are tunable to light wavelengths and intensities (Smirnov *et al.,* 2019). The dielectric behavior of SWCNTs can be examined against wavelength, frequency or energy (Sharma and Jaggi, 2017). Figure 6 is demonstrating the dielectric complex of the real and imaginary parts. The permittivity of SWCNTs, given by the real part, decreases drastically below zero to high negative values in the UV range but increase at visible and near infrared wavelengths to lower negative values. While the real part decreases, the imaginary part increases in the UV region, and they start to reverse direction beyond the UV wavelength range towards the visible and NIR regions. The imaginary part indicates that there is a large loss of energy or absorption of light whereby electrons start to be excited to conduction levels. However, the loss of the imaginary part never tends to zero as is the case of pure dielectric materials, while the permittivity of the real part, though increased, remains negative. This behavior Indicates that SWCNTs demonstrate a ferroelectric and metamaterial properties (Flory, 2011). High negative values of the real part of dielectric in the range of -11000 to -7000 is also observed by Zhang and colleagues. According to Zhang et al., radius and electrical conductivity of the CNT bundles are the main contributors of the real part permittivity negative value (Zhang *et al.,* 2015). The change in conductivity is related to excitation of surface plasmons depending on the illumination of light wavelength in the visible and NIR regime (Smirnov *et al.,* 2019). Li and Liu also obtained a negative real part permittivity of the SWCNT samples and explained that the increase and decrease in the real and imaginary parts of the SWCNTs dielectric constant follow the Drude model of free electron movement (Li and Lue, 2007). Similar results by Smirnov *et al.* showed that with higher augmented light intensities, the real part can, however, increase to positive values (Smirnov *et al.,* 2018). This study pointed out that the real part exhibits resonant behavior that the conductivity cannot be explained

by the simple Drude model but rather by using Drude-Lorentz model combined with the Maxwell-Garnett theory.

Carbon nanotubes have unique optoelectronic features and are intriguingly tunable to light, but they are highly anisotropic because of several parametric variations such as in structure (i.e. chirality angle), diameter, and length, which may explain the variations in their optical and electronic properties. Results in this paper appeal to the build-up of a solid background on these nanodevices and give an insight into the optoelectronic features of SWCNTs that would open the potential for numerous applications.

4. Conclusions

Optical characterization with semi-empirical extrapolation using Tauc/Davis and Max-Planck models can be a powerful tool to reveal significant optical and electronic properties of SWCNTs. The high conductivity and the versatile dielectric behavior are features claiming SWCNTs as the nanomaterial for a futuristic wide range of applications. In addition, analysis of the absorption spectra revealed the successful dispersion and separation of SWCNTs that was achieved using an organic solvent along with simple mechanical processing methods, without incorporating any additives. The parameters of sonication and ultracentrifugation durations and concentration were studied. Higher durations of sonication at lower concentrations yielded the optimum homogeneous dispersion, while the separation of semiconducting nanotubes was validated against absorption intensities and bandgap energies.

Acknowledgments

This research was supported by the Universiti Teknologi PETRONAS, Malaysia, through the Graduate Assistantship (GA) Scheme.

References

Alabsi, S.S., Ahmed, A.Y., Dennis, J.O., Khir, M.H.M., Algamili, A.S., 2020. A review of carbon nanotubes field effect-based biosensors. *IEEE Access*, Volume 8, pp. 69509–69521

Arai, T., 2010. 8.2.16.1 Lewis base catalysis. *Science of Synthesis Knowledge,* Volume 4, p. 224

Arbab, A.I., 2019. On the optical conductivity. *Optik*, Volume 194, p. 163067

Attal, S., Thiruvengadathan, R., Regev, O., 2006. Determination of the concentration of single-walled carbon nanotubes in aqueous dispersions using UV-visible absorption spectroscopy. *Analytical Chemistry*, Volume 78(23), pp. 8098–8104

Ba Hashwan, S.S., Fatin, M.F., Ruslinda, A.R., Md Arshad, M.K., Hashim, U., Ayub, R.M., 2015. Functionalization of multi wall carbon nanotubes using nitric acid oxidation. *Applied Mechanics and Materials*, Volume 754–755, pp. 1156–1160

Barman, S.N., Lemieux, M.C., Baek, J., Rivera, R., Bao, Z., 2010. Effects of dispersion conditions of single-walled carbon nanotubes on the electrical characteristics of thin film network transistors. *ACS Applied Materials and Interfaces*, Volume 2(9), pp. 2672–2678

Berwal, N., Dhankhar, S., Sharma, P., Kundu, R.S., Punia, R., Kishore, N., 2017. Physical, structural and optical characterization of silicate modified bismuth-borate-tellurite glasses. *Journal of Molecular Structure*, Volume 1127, pp. 636–644

Blancon, J., 2015. *Optical absorption and electronic properties of individual carbon nanotubes To cite this version : e par carbone individuels*. Master's Thesis, Graduate Program, Université Claude Bernard Lyon 1, France

Bouazza, A., Bassaid, S., Daho, B., Messori, M., Dehbi, A., 2021. Synthesis and characterization of a composite organic semiconductor (curcumin-paracetamol/TiO2). *Polymers and Polymer Composites*, Volume 29(5), pp. 417–426

Cheung, W., Patel, M., Ma, Y., Chen, Y., Xie, Q., Lockard, J.V., Gao, Y., He, H., 2016. π-Plasmon absorption of carbon nanotubes for the selective and sensitive detection of Fe3+ ions. *Chemical Science*, Volume 7(8), pp. 5192–5199

Chiodarelli, N., De Volder, M., 2019. High-throughput and consistent production of aqueous suspensions of Single-Wall Carbon Nanotubes. *Carbon*, Volume 145, pp. 757–763

El-Moussawi, Z., Nourdine, A., Medlej, H., Hamieh, T., Chenevier, P., Flandin, L., 2019. Fine tuning of optoelectronic properties of single-walled carbon nanotubes from conductors to semiconductors. *Carbon*, Volume 153, pp. 337–346

Engtrakul, C., Davis, M.F., Gennett, T., Dillon, A.C., Jones, K.M., Heben, M.J., 2005. Protonation of carbon single-walled nanotubes studied using13C and1H-13C cross polarization nuclear magnetic resonance and Raman spectroscopies. *Journal of the American Chemical Society*, Volume 127(49), pp. 17548–17555

Eremina, V.A., Obraztsov, P.A., Fedotov, P.V., Chernov, A.I., Obraztsova, E.D., 2017. Separation and optical identification of semiconducting and metallic single-walled carbon nanotubes. *Physica Status Solidi (B) Basic Research*, Volume 254(5), p. 1600659

Farbod, M., Zilaie, A., Kazeminezhad, I., 2017. Advanced materials and devices carbon nanotubes length optimization for preparation of improved transparent and conducting thin fi lm substrates. *Journal of Science: Advanced Materials and Devices*, Volume 2(1), pp. 99–104

Flory, F., 2011. Optical properties of nanostructured materials: a review. *Journal of Nanophotonics*, Volume 5(1), p. 052502

Gharbavi, K., Badehian, H., 2015. Optical properties of armchair (7,7) single walled carbon nanotubes. *AIP Advances*, Volume 5(7), p. 077155

Gomulya, W., Costanzo, G.D., De Carvalho, E.J.F., Bisri, S.Z., Derenskyi, V., Fritsch, M., Fröhlich, N., Allard, S., Gordiichuk, P., Herrmann, A., Marrink, S.J., Dos Santos, M.C., Scherf, U., Loi, M.A., 2013. Semiconducting single-walled carbon nanotubes on demand by polymer wrapping. *Advanced Materials*, Volume 25(21), pp. 2948–2956

He, X., Gao, W., Li, B., Zhang, Q., 2016. Wafer-scale monodomain films of spontaneously aligned single-walled carbon nanotubes. *Nature Nanotechnology,* Volume 11, pp. 633–638

Jiang, Y., Song, H., Xu, R., 2018. Research on the dispersion of carbon nanotubes by ultrasonic oscillation, surfactant and centrifugation respectively and fiscal policies for its industrial development. *Ultrasonics Sonochemistry*, Volume 48, pp. 30–38

Johan, M.R., Suhaimy, S.H.M., Yusof, Y., 2014. Physico-chemical studies of cuprous oxide (Cu 2 O) nanoparticles coated on amorphous carbon nanotubes (α-CNTs). *Applied Surface Science*, Volume 289, pp. 450–454

Kawale, S.S., Afre, R., Sharon, M., Bhosale, C.H., Sharon, M., 2016. *Carbon nanotube : An indirect ~ 0 eV band gap material* Volume 11(7), pp. 3546–3550

Kim, S.L., Choi, K., Tazebay, A., Yu, C., 2014. Flexible power fabrics made of carbon nanotubes for harvesting thermoelectricity. *ACS Nano*, Volume 8(3), pp. 2377–2386

Kozlowska, M., Meyer, B., Rodziewicz, P., 2019. Single-walled carbon nanotubes in tetrahydrofuran solution: microsolvation from first-principles calculations. *Journal of Molecular Modeling*, Volume 25(7), p. 206

Kuwahara, Y., Hirai, T., Saito, T., 2018. Effects of tube diameter and length on transparent conductivity of single-walled carbon nanotube network films. *Journal of Nanomaterials*, Volume 2018, p. 5393290

Li, X., Zhu, H., Wei, J., Wang, K., Xu, E., Li, Z., Wu, D., 2009. Determination of band gaps of self-assembled carbon nanotube films using Tauc/Davis-Mott model. *Applied Physics A: Materials Science and Processing*, Volume 97(2), pp. 341–344

Li, Y.H., and Lue, J.T., 2007. Dielectric constants of single-wall carbon nanotubes at various frequencies. *Journal of Nanoscience and Nanotechnology*, Volume 7(9), pp. 3185–3188

Mougel, J., Adda, C., Bertoncini, P., Capron, I., Cathala, B., Chauvet, O., 2016. Highly e ffi cient and predictable noncovalent dispersion of single- walled and multi-walled carbon nanotubes by cellulose nanocrystals. *Journal of Physical Chemistry C,* Volume 120(39), pp. 22694–22701

Mousavi, H., 2012. Optical conductivity of carbon nanotubes. *Optics Communications*, Volume 285(13–14), pp. 3137–3139

Murali, S., Perumal, S., 2018. Synthesis of nanotubes under carbon environment at low temperature using hydrothermal method. *Optik*, Volume 162, pp. 81–85

Nguyen, T.T., Nguyen, S.U., Phuong, D.T., Nguyen, D.C., Mai, A.T., 2011. Dispersion of denatured carbon nanotubes by using a dimethylformamide solution. *Advances in Natural Sciences: Nanoscience and Nanotechnology*, Volume 2(3), p. 035015

Nguyen, V. H., Shim, J. J., 2015. Green synthesis and characterization of carbon nanotubes/polyaniline nanocomposites. *Journal of Spectroscopy*, Volume 2015, p. 297804

Njuguna, J., Vanli, O.A., Liang, R., 2015. A review of spectral methods for dispersion characterization of carbon nanotubes in aqueous suspensions. *Journal of Spectroscopy*, Volume 2015, p. 463156

Ong, P.L., Euler, W.B., Levitsky, I. A., 2010. Hybrid solar cells based on single-walled carbon nanotubes/Si heterojunctions. *Nanotechnology*, Volume 21(10), p. 105203

Qiu, M., Xie, Y., Gao, X., Li, J., Deng, Y., Guan, D., Ma, L., Yuan, C., 2016. Band gap opening and semiconductor-metal phase transition in (n, n) single-walled carbon nanotubes with distinctive boron-nitrogen line defect. *Physical Chemistry Chemical Physics*, Volume 18(6), pp. 4643–4651

Rance, G.A., Marsh, D.H., Nicholas, R.J., Khlobystov, A.N., 2010. UV-vis absorption spectroscopy of carbon nanotubes: Relationship between the π-electron plasmon and nanotube diameter. *Chemical Physics Letters*, Volume 493(1–3), pp. 19–23

Saad, I. Ben, Hannachi, N., Roisnel, T., Hlel, F., 2019. Optical, UV-Vis spectroscopy studies, electrical and dielectric properties of transition metal-based of the novel organic-inorganic hybrid (C6 H10 N2)(Hg2Cl5)2.3H2O. *Journal of Advanced Dielectrics*, Volume 9(5), pp. 1–15

Setyopratomo, P., Wulan, P.P.D.K., Sudibandriyo, M., 2018. The effect of metal loading on the performance of tri-metallic supported catalyst for carbon nanotubes synthesis from liquefied petroleum gas. *International Journal of Technology*, Volume 9(1), pp. 120–129

Sharma, D., Jaggi, N., 2017. Static refractive index engineering of a singlewalled carbon nanotube through co-doping: A theoretical study. *Optik*, Volume 131, pp. 267–272

Sharma, P., Katyal, S. C., 2007. Determination of optical parameters of a-(As2Se 3)90Ge10 thin film. *Journal of Physics D: Applied Physics*, Volume 40(7), pp. 2115–2120

Simien, D., Fagan, J.A., Luo, W., Douglas, J.F., Migler, K., Obrzut, J., 2008. Influence of nanotube length on the optical and conductivity properties of thin single-wall carbon nanotube networks. *ACS Nano*, Volume 2(9), pp. 1879–1884

Smirnov, S., Anoshkin, I.V., Demchenko, P., Gomon, D., Lioubtchenko, D.V., Khodzitsky, M., Oberhammer, J., 2018. Optically controlled dielectric properties of single-walled carbon nanotubes for terahertz wave applications. *Nanoscale*, Volume 10(26), pp. 12291–12296

Smirnov, S., Anoshkin, I.V., Generalov, A., Lioubtchenko, D.V., Oberhammer, J., 2019. Wavelength-dependent photoconductivity of single-walled carbon nanotube layers. *RSC Advances*, Volume 9(26), pp. 14677–14682

Sudibandriyo, M., Wulan, P.P.D.K., Prasodjo, P., 2015. Adsorption capacity and its dynamic behavior of the hydrogen storage on carbon nanotubes. *International Journal of Technology*, Volume 6(7), pp. 1128–1136

Sun, J., 2011. Stability and electronic structures of single-walled AlP nanotubes by first principle study. *Procedia Engineering*, Volume 15, pp. 5062–5066

Tan, K.H., Ahmad, R., Leo, B.F., Yew, M.C., Ang, B.C., Johan, M.R., 2012. Physico-chemical studies of amorphous carbon nanotubes synthesized at low temperature. *Materials Research Bulletin*, Volume 47(8), pp. 1849–1854

Tang, J., Cao, Q., Tulevski, G., Jenkins, K.A., Nela, L., Farmer, D.B., Han, S.J., 2018. Flexible CMOS integrated circuits based on carbon nanotubes with sub-10 ns stage delays. *Nature Electronics*, Volume 1(3), pp. 191–196

Tan, W.H., Lee, S.L., Ng, J., Chong, W.W.F., Chong, C.T., 2016. Characterization of carbon nanotubes synthesized from hydrocarbon-rich flame. *International Journal of Technology*, Volume 7(2), pp. 343–351

Tsapenko, A.P., Goldt, A.E., Shulga, E., Popov, Z.I., Maslakov, K.I., Anisimov, A.S., Sorokin, P. B., Nasibulin, A.G., 2018. Highly conductive and transparent films of HAuCl4-doped single-walled carbon nanotubes for flexible applications. *Carbon*, Volume 130, pp. 448–457

Venkataraman, A., Amadi, E.V., Chen, Y., Papadopoulos, C., 2019. Carbon nanotube assembly and integration for applications. *Nanoscale Research Letters*, Volume 14(1), p. 220

Wang, J., Lei, T., 2020. Separation of semiconducting carbon nanotubes using conjugated polymer wrapping. *Polymers*, Volume 12(7), pp. 1–29

Wang, W., Xu, J., Zhang, Y., Li, G., 2017. First-Principles Study of Electronic Structure and Optical Properties of Silicon/Carbon Nanotube. *Computational Chemistry*, Volume 05(04), pp. 159–171

Yang, M-c., Li, M-y, Luo, S., Liang, R., 2016. Real-time monitoring of carbon nanotube dispersion using dynamic light scattering and UV-vis spectroscopy. *International Journal of Advanced Manufacturing Technology*, Volume 82(1–4), pp. 361–367

Zhang, W., Xiong, H., Wang, S., Li, M., Gu, Y., 2015. Negative permittivity behavior of aligned carbon nanotube films. *Applied Physics Letters*, Volume 106(18), pp. 3–8